
Downlink Compression Improves Top_K Sparsification

William Zou
University of Waterloo
wyzou@uwaterloo.ca

Hans De Sterck
University of Waterloo
hans.desterck@uwaterloo.ca

Jun Liu
University of Waterloo
j.liu@uwaterloo.ca

Abstract

Training large neural networks is time consuming. To speed up the process, distributed training is often used. One of the largest bottlenecks in distributed training is communicating gradients across different nodes. Different gradient compression techniques have been proposed to alleviate the communication bottleneck, including top_K gradient sparsification, which truncates the gradient to the largest K components before sending it to other nodes. While some authors have investigated top_K gradient sparsification in the parameter-server framework by applying top_K compression in both the worker-to-server (uplink) and server-to-worker (downlink) direction, the currently accepted belief says that adding extra compression degrades the convergence of the model. We demonstrate, on the contrary, that adding downlink compression can potentially improve the performance of top_K sparsification: not only does it reduce the amount of communication per step, but also, counter-intuitively, can improve the upper bound in the convergence analysis. To show this, we revisit non-convex convergence analysis of top_K stochastic gradient descent (SGD) and extend it from the unidirectional to the bidirectional setting. We also remove a restriction of the previous analysis that requires unrealistically large values of K . We experimentally evaluate bidirectional top_K SGD against unidirectional top_K SGD and show that models trained with bidirectional top_K SGD will perform as well as models trained with unidirectional top_K SGD while yielding significant communication benefits for large numbers of workers.

1 Introduction

Deep neural networks trained on large datasets are known to achieve state-of-the-art performance in accuracy. However, the large size of the models and datasets severely impacts the training time of the model. To decrease the training time, distributed machine training techniques are often used, which in recent years have involved scaling stochastic gradient descent (SGD) to multiple processes [10, 4].

The standard way to scale SGD on multiple processes is through data parallelism where the training set is split across n different processes [10]. Each node will calculate a stochastic gradient from their allocated data independently and in parallel. The nodes then communicate the gradient with each other before updating model parameters. We want to minimize the weighted average of N different functions $(F^q)_{q=1}^N : \mathbb{R}^d \rightarrow \mathbb{R}$ across N nodes

$$\min_{w \in \mathbb{R}^d} F(w) \triangleq \sum_{q=1}^N p_q F^q(w), \quad (1)$$

by applying the iteration

$$w_t = w_{t-1} - \alpha_t \sum_{q=1}^N p_q g^q(w_{t-1}, \xi_{t-1}^q), \quad (2)$$

where w_t is the model parameters at iteration t , $g^q(\cdot, \cdot)$ is a stochastic gradient of F , α_t is the step size at time t , and ξ_{t-1}^q represents a local sample, similar to how it is used in [6].

Communication between nodes is one of the largest bottleneck in distributed machine learning [22]. Most efforts in increasing the performance speed of distributed learning come from reducing this bottleneck. One of the most well-studied compression technique is sparsification, which focuses on reducing communication between worker nodes by sending only a sparse subset of the gradient [4, 22]. The most popular of these methods is top_K gradient sparsification, which truncates the gradient to the largest K components by magnitude [7, 22]. top_K gradient sparsification was originally only used during the worker-to-server (uplink) communication of the parameter-server framework [17], since the gradient sent by the server is sparse if the number of participating workers is low.

Due to the increased number of workers used in distributed training, Sattler *et al.* recommended adding top_K gradient sparsification during server-to-worker (downlink) communication as well, and reported that sparsifying the gradients in both uplink and downlink communication (bidirectional) reduces the final accuracy by at most 3% compared to only using uplink [17]. Theoretical frameworks from Tang *et al.* and Zheng *et al.* have been developed to analyze the convergence of bidirectionally compressed error-compensated SGD, which can be used to analyze bidirectional top_K gradient sparsification [20, 23]. However, these studies suggest that adding downlink sparsification will degrade the convergence of the model [16, 20, 23]. We show that under the theoretical framework provided by Alistarh *et al.* [2], we can construct an upper bound for the non-convex convergence of bidirectional top_K SGD that is potentially smaller than the upper bound of unidirectional top_K SGD.

Related work. To the best of our knowledge, top_K sparsification was first proposed by Aji and Heafield [1]. Alistarh *et al.* and Stich *et al.* later analyzed the convergence rate of unidirectional top_K sparsification, and showed that the scheme converges at the same rate as vanilla SGD [2, 19].

Bidirectional top_K SGD has been used in the Federated Learning setting. Sattler *et al.* evaluated communication protocols for Federated Learning, and suggested adding top_K sparsification in the server-to-worker direction [17]. They reported that using bidirectional top_K SGD did not destabilize the training as much as using bidirectional signSGD.

Beyond applications in Federated Learning, theoretical frameworks to evaluate the convergence rate of bidirectional biased compression techniques with error-feedback framework have been developed in [20, 23]. As far as we know, Tang *et al.* was the first to have developed convergence analysis for bidirectional error feedback SGD compatible with any compression technique, and showed the same convergence rate as SGD under certain assumptions [20]. Zheng *et al.* developed a similar theoretical framework to Tang *et al.* independently [23]. Since then, there have been theoretical frameworks developed for variations of bidirectional algorithms [14, 15]. Liu *et al.* developed DORE, which compresses and sends gradient residuals [14], and Philippenko and Dieuleveut introduced the Artemis framework to analyze unbiased compressors [15]. To the best of our knowledge, no bidirectional compression framework has shown that adding downlink compression can improve the convergence bound of the unidirectional compression framework.

Contributions. To summarize, the contributions of our paper are as follows:

- **Showing downlink compression can improve constants in the convergence bound of top_K SGD:** We extend the convergence analysis of Alistarh *et al.* to bidirectional top_K SGD [2], and show that bidirectional top_K has the same convergence rate as unidirectional top_K SGD but with constants that may be smaller.
- **Generalization of non-convex analysis of top_K SGD:** We fix a major limitation of the original unidirectional top_K non-convex analysis in [2] so that it works for $K < \frac{1}{2}d$, where d is the size of the gradient. Note that $K \geq \frac{1}{2}d$ means that one can compress the gradient by a factor of at most 2, which is not practical.
- **Estimate of compression factor achieved by downlink compression:** We provide an empirical estimate of the compression factor achieved by downlink sparsification, and show that top_K SGD can provide significant communication benefits when the number of workers is large.

2 Bidirectional Top_K SGD Algorithm

We describe top_K SGD and bidirectional top_K SGD in Algorithms 1 and 2. For both algorithms, during the t -th iteration, each worker q calculates the stochastic gradient $g^q(w_{t-1}, \xi_t^q)$, compresses the error-compensated value $\alpha_{t-1}g^q(w_{t-1}, \xi_t^q) + \epsilon_{t-1}^q$, updates the local error term with $\epsilon_{t-1}^q = a_t^q - \text{Top}_K(a_t^q)$, then sends the error-compensated value to the server.

The server aggregates all error-compensated values $\sum_{q=1}^N p_q \text{Top}_K(a_t^q)$. In unidirectional top_K SGD, this values is sent directly back to each individual worker. In bidirectional top_K SGD, the server compresses the error-compensated value $\sum_{q=1}^N p_q \text{Top}_K(a_t^q) + \delta_{t-1}$, updates the global error term with $\delta_t = g_t - \text{Top}_K(g_t)$, before sending the error-compensated value back to each individual worker, where it will be used to update local models.

The main benefit of bidirectional sparsification is the communication saved in the server-to-worker direction. Note that $\sum_{q=1}^N p_q \text{Top}_K(a_t^q)$ is a sparse vector when $N \ll D$. We investigate the communication saved in more detail in Section 4.2.

Algorithm 1: Unidirectional Top_K SGD

Input: Stochastic Gradient Oracle $g^q(\cdot; \cdot)$,
learning rate sequence $\{\alpha_t\}_{t \geq 0}$,
probability vector (p_0, \dots, p_N)

- 1 Initialize $w_0 \in \mathbb{R}^d; \epsilon_0^q = 0 \in \mathbb{R}^d; t = 1$;
- 2 **while** $t \geq 1$ **do**
- 3 **On worker q :**
- 4 $a_t^q \leftarrow \epsilon_{t-1}^q + \alpha_{t-1}g^q(w_{t-1}, \xi_{t-1}^q)$;
- 5 $\epsilon_t^q \leftarrow a_t^q - \text{Top}_K(a_t^q)$;
- 6 SEND($\text{Top}_K(a_t^q)$, server);
- 7 **On server:**
- 8 **for every worker q do**
- 9 | RECV($\text{Top}_K(a_t^q)$, q);
- 10 **end**
- 11 $g_t \leftarrow \sum_{q=1}^N p_q \text{Top}_K(a_t^q)$;
- 12 **for every client q do**
- 13 | SEND(g_t , q);
- 14 **end**
- 15 **On worker q :**
- 16 RECV(g_t , server);
- 17 $w_t \leftarrow w_{t-1} - g_t$;
- 18 $t = t + 1$;
- 19 **end**

Algorithm 2: Bidirectional Top_K SGD

Input: Stochastic Gradient Oracle $g^q(\cdot; \cdot)$,
learning rate sequence $\{\alpha_t\}_{t \geq 0}$,
probability vector (p_0, \dots, p_N)

- 1 Initialize $w_0 \in \mathbb{R}^d; \epsilon_0^q = 0 \in \mathbb{R}^d$;
 $\delta_0 = 0 \in \mathbb{R}^d; t = 1$;
- 2 **while** $t \geq 1$ **do**
- 3 **On worker q :**
- 4 $a_t^q \leftarrow \epsilon_{t-1}^q + \alpha_{t-1}g^q(w_{t-1}, \xi_{t-1}^q)$;
- 5 $\epsilon_t^q \leftarrow a_t^q - \text{Top}_K(a_t^q)$;
- 6 SEND($\text{Top}_K(a_t^q)$, server);
- 7 **On server:**
- 8 **for every worker q do**
- 9 | RECV($\text{Top}_K(a_t^q)$, q);
- 10 **end**
- 11 $g_t \leftarrow \sum_{q=1}^N p_q \text{Top}_K(a_t^q) + \delta_{t-1}$;
- 12 $\delta_t \leftarrow g_t - \text{Top}_K(g_t)$;
- 13 **for every client q do**
- 14 | SEND($\text{Top}_K(g_t)$, q);
- 15 **end**
- 16 **On worker q :**
- 17 RECV($\text{Top}_K(g_t)$, server);
- 18 $w_t \leftarrow w_{t-1} - \text{Top}_K(g_t)$;
- 19 $t = t + 1$;
- 20 **end**

3 Convergence Analysis of Bidirectional Top_K SGD

In this section, we analyze the convergence of the stochastic sequence $\{w_t\}_{t \geq 0}$ in Algorithm 2 in the non-convex setting. We follow the proof structure created by Alistarh *et al* [2] for analyzing unidirectional top_K sparsification.

3.1 Analytic Assumptions

Assumption 3.1 (Existence of lower bound). *There exists some constant F^* such that $F(w) \geq F^*$ for all $w \in \mathbb{R}^d$.*

Assumption 3.2 (Biased compressor guarantee). *There exists some $\gamma \in (0, 1)$ such that*

$$\|\text{Top}_K(w) - w\|_2^2 \leq (1 - \gamma)\|w\|_2^2 \quad \forall w \in \mathbb{R}^d. \quad (3)$$

This assumption is commonly used with biased compression schemes [5, 11]. We mention that we can always find a γ value to satisfy this assumption for top_K , since we know

$$\|\text{Top}_K(w) - w\|_2^2 \leq \frac{d-K}{d} \|w\|_2^2, \quad (4)$$

where d is the dimension of the gradient.

Assumption 3.3 (Lipschitz continuous gradient). F is continuously differentiable and the gradient $\nabla F : \mathbb{R}^d \rightarrow \mathbb{R}^d$ is Lipschitz continuous with constant $L > 0$, i.e.,

$$\|\nabla F(w) - \nabla F(v)\|_2 \leq L\|w - v\|_2 \quad \forall w, v \in \mathbb{R}^d.$$

Assumption 3.4 (First and second moments). The objective function and Algorithm 2 satisfy the following:

$$\mathbb{E}\left[\sum_{q=1}^N p_q g^q(w, \xi_t^q)\right] = \sum_{q=1}^N p_q \nabla F^q(w) \quad \forall w \in \mathbb{R}^d, \forall t \in \mathbb{N}, \quad (5)$$

and

$$\mathbb{E}\left[\left\|\sum_{q=1}^N p_q g^q(w, \xi_t^q)\right\|_2^2\right] \leq M \quad \forall w \in \mathbb{R}^d, \forall t \in \mathbb{N}, \quad (6)$$

where $\mathbb{E}[\cdot]$ is taken with respect to the joint distribution of $\{\xi_t^1, \xi_t^2, \dots, \xi_t^N\}$.

Assumption 3.5. Given a sequence of iterates $\{w_t\}$, there exists $\rho > 0$ such that

$$\begin{aligned} & \left\| \text{Top}_K(\delta_{t-1} + \sum_{q=1}^N p_q a_t^q) - \text{Top}_K(\delta_{t-1} + \sum_{q=1}^N \text{Top}_K(p_q a_t^q)) \right\|_2 \\ & \leq \rho \|\alpha_{t-1} \sum_{q=1}^N p_q g^q(w_{t-1}, \xi_{t-1}^q)\|_2 \quad \forall t \in \mathbb{N}. \end{aligned}$$

Assumption 3.5 is similar to the assumption made by Alistarh *et al* [2], which is described in Assumption 3.6. The authors in [2] explain this as a bound on the variance of the local gradients with respect to the global variance. We discuss this assumption in more detail in our toy example in supplemental material A.1, and compare it to Assumption 3.6 in our discussion in Section 3.2.

3.2 Convergence Bound

We present the main theorem for this section.

Theorem 3.1. Under Assumptions 3.1–3.5, if a learning rate sequence $\{\alpha_t\}_{t \geq 0}$ and constant $\lambda \in (0, \frac{1-\gamma}{\gamma})$ are chosen such that there exists constant $D > 0$ with

$$\frac{1}{1-\gamma} \sum_{i=1}^t ((1+\lambda)(1-\gamma))^i \frac{\alpha_{t-i}^2}{\alpha_t} \leq D, \quad \forall t \geq 1, \quad (7)$$

then running Algorithm 2 for T iterations will give

$$\begin{aligned} \frac{1}{\sum_{t=0}^T \alpha_t} \sum_{t=0}^T \alpha_t \mathbb{E}[\|\nabla F(w_t)\|_2^2] & \leq \frac{2}{\sum_{t=0}^T \alpha_t} (F(w_0) - F^*) \\ & + \left(LM + \frac{L^2 MD(\sqrt{1-\gamma} + \rho)^2}{\lambda} \right) \frac{\sum_{t=0}^T \alpha_t^2}{\sum_{t=0}^T \alpha_t}. \end{aligned} \quad (8)$$

In order for the upper bound in (8) to converge to zero we need $\sum_{t=1}^{\infty} \alpha_t = \infty$ and $\sum_{t=1}^{\infty} \alpha_t^2 < \infty$. We can choose the stepsize sequence $\alpha_t = \frac{1}{(t+1)^\theta}$, $\frac{1}{2} < \theta \leq 1$. Finally, we need to check if the sequence can satisfy (7).

We can ensure (7) is bounded by requiring $(1 + \lambda)(1 - \gamma) < 1$. We can always find a λ that satisfies the inequality, since $\gamma \in (0, 1)$ from Assumption 3.2. It is then easy to see that (7) is satisfied, since the exponential term dominates the polynomial term.

Remark. Changing Assumption 3.5 to Assumption 3.6 gives unidirectional top_K SGD the same convergence bound as bidirectional top_K SGD, but with ρ replaced by $\hat{\rho}$.

Assumption 3.6. *Given a sequence of iterates $\{w_t\}$, there exists $\rho > 0$ such that*

$$\|\text{Top}_K(\sum_{q=1}^N p_q a_t^q) - \sum_{q=1}^N \text{Top}_K(p_q a_t^q)\|_2 \leq \hat{\rho} \|\alpha_{t-1} \sum_{q=1}^N p_q g^q(w_{t-1}, \xi_{t-1}^q)\|_2 \quad \forall t \in \mathbb{N}, \quad (9)$$

Bidirectional top_K SGD has the same convergence bound as unidirectional top_K SGD. If we choose the step size to be $\alpha_t = \frac{1}{(t+1)^{1/2+\epsilon}}$, where ϵ is an arbitrarily small number, the bound in Theorem 3.1 will approach 0 at $O(1/\sqrt{T})$. We compare the performance of bidirectional to unidirectional top_K SGD in Section 4, and estimate the values of the constants in their convergence bound. Intuitively, $\rho < \tilde{\rho}$ if the unidirectional top_K update step is noisy, since applying downlink top_K compression can potentially dampen noise. We provide a toy example to demonstrate this in supplemental material A.1.

3.3 Proof

Similar to other error-compensated SGD analysis [2, 11], we consider an error-corrected sequence

$$\tilde{w}_t = w_t - \sum_{q=1}^N p_q \epsilon_t^q - \delta_t, \quad (10)$$

where \tilde{w}_t is the model parameter vector after accounting for the error term stored on all workers and server. To get the non-convex convergence bound, we apply the standard proof of SGD to \tilde{w}_t , and show that $\tilde{w}_t \approx w_t$ and $\nabla F(\tilde{w}_t) \approx \nabla F(w_t)$. We use the following lemmas to construct the convergence bound.

Lemma 3.2. *Let $\{\tilde{w}_t\}_{t \geq 0}$ be defined in (10), and $\{w_t\}_{t \geq 0}$, $\{\alpha_t\}_{t \geq 0}$, and p_i for $1 \leq i \leq N$ be defined in Algorithm 2. Then*

$$\tilde{w}_t = \tilde{w}_{t-1} - \alpha_{t-1} \sum_{q=1}^N p_q g^q(w_{t-1}, \xi_{t-1}^q). \quad (11)$$

Proof. We have

$$\begin{aligned} \tilde{w}_t &= w_t - \delta_t - \sum_{q=1}^N p_q \epsilon_t^q \\ &= w_{t-1} - \delta_{t-1} - \sum_{q=1}^N p_q a_t^q \\ &= \tilde{w}_{t-1} + \sum_{q=1}^N p_q \epsilon_{t-1}^q + \delta_{t-1} - \delta_{t-1} - \sum_{q=1}^N p_q a_t^q \\ &= \tilde{w}_{t-1} - \alpha_{t-1} \sum_{q=1}^N p_q g^q(w_{t-1}, \xi_{t-1}^q). \end{aligned} \quad (12)$$

□

We use the previous lemma and Assumptions 3.2 and 3.5 to bound the difference between the error-corrected sequence $\{\tilde{w}_t\}$ and $\{w_t\}$.

Lemma 3.3. Let $\{w_t\}_{t \geq 0}$ be defined by Algorithm 2, and $\{\tilde{w}_t\}_{t \geq 0}$ be defined by (10). Under Assumptions 3.2 and 3.5, we have

$$\|w_t - \tilde{w}_t\|_2 \leq \frac{1}{\lambda}(\sqrt{1-\gamma} + \rho)^2 \frac{1}{1-\gamma} \sum_{i=1}^t ((1+\lambda)(1-\gamma))^i \|\tilde{w}_{t-i+1} - \tilde{w}_{t-i}\|_2^2, \quad (13)$$

where one can choose the constant $\lambda \in (0, \frac{\gamma}{1-\gamma})$.

Proof. Applying Lemma 3.2 and the iterative relation of sequence $\{w_t\}_{t \geq 0}$ defined in Algorithms 2, we get:

$$\begin{aligned} \|w_t - \tilde{w}_t\|_2 &= \|w_{t-1} - \tilde{w}_{t-1} + \alpha_{t-1} \sum_{q=1}^N p_q g^q(w_{t-1}, \xi_{t-1}^q) - \\ &\quad \text{Top}_K(\sum_{q=1}^N p_q \text{Top}_K(a_t^q) + \delta_{t-1})\|_2 \\ &= \|\delta_{t-1} + \sum_{q=1}^N p_q \epsilon_{t-1}^q + \alpha_{t-1} \sum_{q=1}^N p_q g^q(w_{t-1}, \xi_{t-1}^q) - \\ &\quad \text{Top}_K(\sum_{q=1}^N p_q \text{Top}_K(a_t^q) + \delta_{t-1})\|_2 \\ &\leq \|\delta_{t-1} + \sum_{q=1}^N p_q a_t^q - \text{Top}_K(\delta_{t-1} + \sum_{q=1}^N p_q a_t^q)\|_2 + \\ &\quad \|\text{Top}_K(\delta_{t-1} + \sum_{q=1}^N p_q a_t^q) - \text{Top}_K(\delta_{t-1} + \sum_{q=1}^N \text{Top}_K(p_q a_t^q))\|_2. \end{aligned} \quad (14)$$

Using Assumption 3.2 and 3.5, we get

$$\begin{aligned} \|w_t - \tilde{w}_t\|_2 &\leq \sqrt{1-\gamma} \|\delta_{t-1} + \sum_{q=1}^N p_q a_t^q\|_2 + \rho \|\alpha_{t-1} \sum_{q=1}^N p_q g(w_{t-1}, \xi_{t-1}^q)\|_2 \\ &\leq \sqrt{1-\gamma} \|\delta_{t-1} + \sum_{q=1}^N p_q \epsilon_{t-1}^q\|_2 + \\ &\quad (\sqrt{1-\gamma} + \rho) \|\alpha_{t-1} \sum_{q=1}^N p_q g(w_{t-1}, \xi_{t-1}^q)\|_2 \\ &\leq \sqrt{1-\gamma} \|w_{t-1} - \tilde{w}_{t-1}\|_2 + (\sqrt{1-\gamma} + \rho) \|\tilde{w}_t - \tilde{w}_{t-1}\|_2, \end{aligned} \quad (15)$$

where the final inequality in (15) is from Lemma 3.2 and the definition of the error-corrected sequence \tilde{w}_t given in (10). Taking the square, we get

$$\begin{aligned} \|w_t - \tilde{w}_t\|_2^2 &\leq (\sqrt{1-\gamma} \|w_{t-1} - \tilde{w}_{t-1}\|_2 + (\sqrt{1-\gamma} + \rho) \|\tilde{w}_t - \tilde{w}_{t-1}\|_2)^2 \\ &\leq (1+\lambda)(1-\gamma) \|w_{t-1} - \tilde{w}_{t-1}\|_2^2 + \\ &\quad (1 + \frac{1}{\lambda})(\sqrt{1-\gamma} + \rho)^2 \|\tilde{w}_t - \tilde{w}_{t-1}\|_2^2, \end{aligned} \quad (16)$$

which holds for any $\lambda > 0$. For reasons that will become clear later, we choose $\lambda \in (0, \frac{\gamma}{1-\gamma})$. Iterating downwards on (16) gives

$$\begin{aligned} \|\tilde{w}_t - w_t\|_2^2 &\leq \sum_{i=1}^t ((1+\lambda)(1-\gamma))^{i-1} (1 + \frac{1}{\lambda})(\sqrt{1-\gamma} + \rho)^2 \|\tilde{w}_{t-i+1} - \tilde{w}_{t-i}\|_2^2 \\ &= \frac{1}{\lambda} (\sqrt{1-\gamma} + \rho)^2 \frac{1}{1-\gamma} \sum_{i=1}^t ((1+\lambda)(1-\gamma))^i \|\tilde{w}_{t-i+1} - \tilde{w}_{t-i}\|_2^2 \end{aligned} \quad (17)$$

□

Using Assumption 3.4, we can bound the expectation of the difference between the error-corrected sequence and the true sequence from Lemma 3.3 with a constant.

Lemma 3.4. *Under the same setting as Lemma 3.3 as well as Assumption 3.4, assume that*

$$\frac{1}{1-\gamma} \sum_{i=1}^t ((1+\lambda)(1-\gamma))^i \frac{\alpha_{t-i}^2}{\alpha_t} \leq D,$$

for some constant $\lambda > 0$ and $D > 0$. Then

$$\mathbb{E}[\|w_t - \tilde{w}_t\|_2^2] \leq \frac{M}{\lambda} (\sqrt{1-\gamma} + \rho)^2 \alpha_t D.$$

We can now prove Theorem 3.1.

Proof. Denote $\mathbb{E}_{\xi_t}[\cdot]$ to be the expectation taken with respect to the joint distribution of $\{\xi_t^1, \xi_t^2, \dots, \xi_t^N\}$ given all random variables before time t . Starting with Assumption 3.3 and taking $\mathbb{E}_{\xi_t}[\cdot]$ on both sides of the inequality, we get

$$\begin{aligned} \mathbb{E}_{\xi_t}[F(\tilde{w}_{t+1})] &\leq F(\tilde{w}_t) + \langle \nabla F(\tilde{w}_t), \mathbb{E}_{\xi_t}[\tilde{w}_{t+1} - \tilde{w}_t] \rangle + \frac{L}{2} \mathbb{E}_{\xi_t}[\|\tilde{w}_{t+1} - \tilde{w}_t\|_2^2] \\ &\leq F(\tilde{w}_t) - \alpha_t \langle \nabla F(\tilde{w}_t), \nabla F(w_t) \rangle + \frac{L\alpha_t^2 M}{2} \\ &\leq F(\tilde{w}_t) - \alpha_t \langle \nabla F(w_t), \nabla F(w_t) \rangle + \frac{L\alpha_t^2 M}{2} + \\ &\quad \alpha_t \langle \nabla F(w_t) - \nabla F(\tilde{w}_t), \nabla F(w_t) \rangle \\ &\leq F(\tilde{w}_t) - \alpha_t \|\nabla F(w_t)\|_2^2 + \frac{L\alpha_t^2 M}{2} + \\ &\quad \frac{\alpha_t}{2} \|\nabla F(w_t)\|_2^2 + \frac{\alpha_t}{2} \|\nabla F(w_t) - \nabla F(\tilde{w}_t)\|_2^2 \\ &\leq F(\tilde{w}_t) - \frac{\alpha_t}{2} \|\nabla F(w_t)\|_2^2 + \frac{L\alpha_t^2 M}{2} + \frac{\alpha_t L^2}{2} \|w_t - \tilde{w}_t\|_2^2. \end{aligned} \tag{18}$$

Taking expectation with respect to the joint distribution of all random variables on both sides of the inequality, and applying Lemma 3.4, we get

$$\mathbb{E}[F(\tilde{w}_{t+1})] \leq \mathbb{E}[F(\tilde{w}_t)] - \frac{\alpha_t}{2} \mathbb{E}[\|\nabla F(w_t)\|_2^2] + \frac{L\alpha_t^2 M}{2} + \frac{\alpha_t^2 L^2 M}{2} \frac{M}{\lambda} (\sqrt{1-\gamma} + \rho)^2 D.$$

Telescoping and rearranging, we get

$$\begin{aligned} \sum_{t=0}^T \alpha_t \mathbb{E}[\|\nabla F(w_t)\|_2^2] &\leq \sum_{t=0}^T 2(\mathbb{E}[F(\tilde{w}_t)] - \mathbb{E}[F(\tilde{w}_{t+1})]) + L\alpha_t^2 M + \\ &\quad \frac{\alpha_t^2 L^2 M D (\sqrt{1-\gamma} + \rho)^2}{\lambda}, \end{aligned}$$

or

$$\begin{aligned} \frac{1}{\sum_{t=0}^T \alpha_t} \sum_{t=0}^T \alpha_t \mathbb{E}[\|\nabla F(w_t)\|_2^2] &\leq \frac{2}{\sum_{t=0}^T \alpha_t} (F(w_0) - F^*) \\ &\quad + \left(LM + \frac{L^2 M D (\sqrt{1-\gamma} + \rho)^2}{\lambda} \right) \frac{\sum_{t=0}^T \alpha_t^2}{\sum_{t=0}^T \alpha_t}, \end{aligned} \tag{19}$$

as desired. \square

4 Experiments

The simulation code used to evaluate bidirectional top_K SGD against unidirectional top_K SGD is built on [3], which is distributed under the MIT license. All the code and models can be found in our

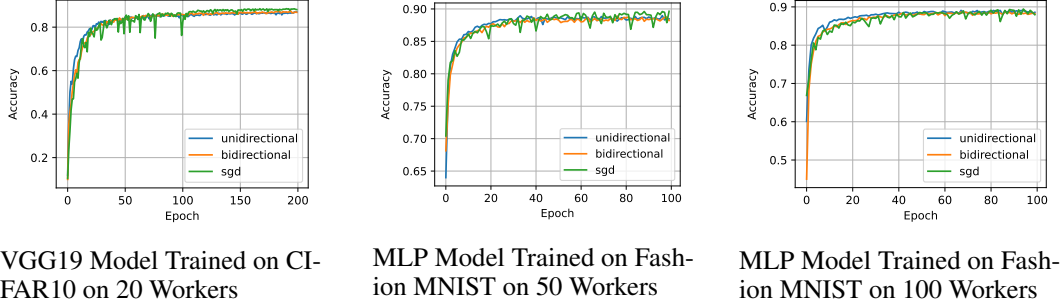


Figure 1: Comparison of testing accuracy.

github repository¹. Experiments are run on the MNIST [8] and the Fashion-MNIST [21] datasets using multilayer perceptrons and convolution neural networks on 20, 50 and 100 workers, as well as on the CIFAR10 dataset [12] using the VGG19 network [18] on 20 workers. For all models we choose $K = d - \lfloor (1 - 0.001)d \rfloor$, where d is the number of parameters in the model. The K value for the uplink and downlink compressor are the same for bidirectional top $_K$ SGD.

MLP and CNN network on MNIST dataset: We train a [784, 64, 10] MLP model from [3] and a CNN model with 2 convolution layers and 1 maxpooling layer from [9]. The MLP and CNN model has 50890 and 1199882 parameters respectively. The MNIST dataset contains 60000 train and 10000 28×28 test images. We randomly split the 60000 elements of the training set into equal size sets and assign each to a worker. Each minibatch size is set to 10 for all models regardless of number of workers participating, and the models are trained for 100 epochs with SGD, unidirectional top $_K$ SGD, and bidirectional top $_K$ SGD. The learning rates for SGD, unidirectional top $_K$ SGD, and bidirectional top $_K$ SGD are tuned separately from 0.01 to 0.25 with step increase of 0.01, unlike previous bidirectional compression experiments, which use the same learning rate [17, 20]. We include the optimum learning rate of the models in Table 2.

MLP and CNN network on Fashion-MNIST dataset: We also train a CNN network with 2 convolution layers and 2 max-pooling layer from [3], and a [784, 256, 128, 64, 10] MLP network. The MLP network has 242762 parameters and the CNN network has 29034 parameters. Similar to the MNIST dataset, the Fashion-MNIST dataset contains 60000 train and 10000 28×28 test images. We train the models using the same setup as our MNIST models, and include the optimum learning rate in Table 2.

VGG19 on CIFAR10 dataset: Finally, we trained a VGG19 network from [13] with 20040522 parameters on the CIFAR10 dataset with 20 workers. The model is trained with batch size 100 for 200 epochs. We tune the learning rate of the VGG19 network trained with SGD on learning rates 0.01, 0.02, 0.05 and 0.1, and use this learning rate for our VGG network trained with unidirectional and bidirectional top $_K$ SGD.

We include the results for training loss and testing accuracy in Figures 1 and 2. A more comprehensive set of test results for training loss and testing accuracy is in supplemental material A.3.1. The results show that bidirectional top $_K$ SGD and unidirectional top $_K$ SGD will achieve similar test accuracy and training loss in the same number of epochs, consistent with our theoretical results that bidirectional and unidirectional top $_K$ SGD have similar convergence rate.

4.1 Convergence Bound Constants

We estimate the constants ρ and $\hat{\rho}$ from the convergence bound of unidirectional and bidirectional top $_K$ SGD in Theorem 3.1, and plot them in Figure 3. We include plots for the rest of the tests in supplemental material A.3.2, and summarize the estimated ρ and $\hat{\rho}$ values of all tests in Table 1. We see that the ρ values for bidirectional top $_K$ SGD are consistently much smaller than the $\hat{\rho}$ values for unidirectional top $_K$ SGD. We also plot the maximum $1 - \gamma$ values in each epoch for bidirectional and unidirectional top $_K$ SGD in supplemental material A.3.3, and mention that the values are approximately the same for both compression schemes. The smaller constant ρ indicate

¹<https://github.com/wyxzou/Federated-Learning-PyTorch>

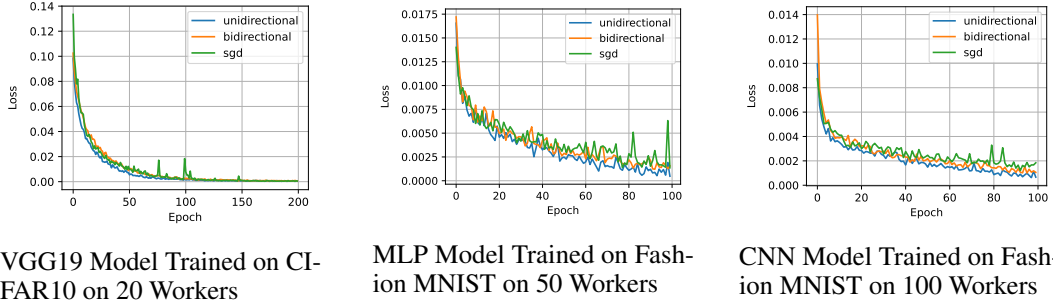


Figure 2: Comparison of training loss.

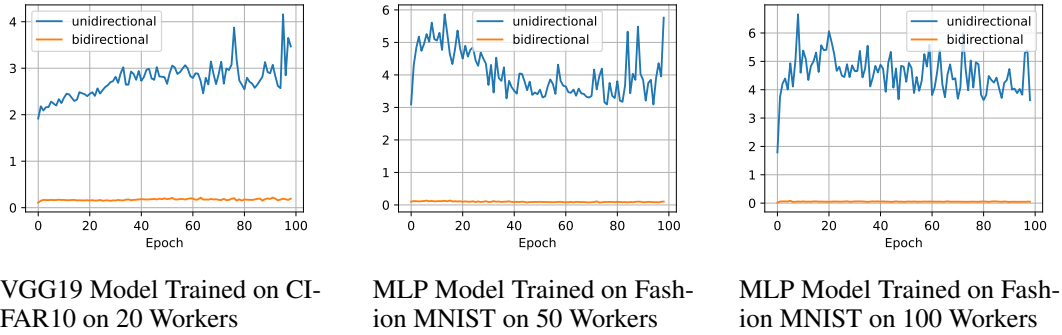


Figure 3: Largest ρ and $\hat{\rho}$ value in each epoch.

that the convergence bound for bidirectional top_K SGD could potentially be much smaller than the convergence bound for unidirectional top_K SGD.

Table 1: Maximum $\hat{\rho}$ and ρ value of trained models across all epochs.

Dataset	Model	Workers	$\hat{\rho}$	ρ
Fashion MNIST	MLP	20	21.78	0.60
		50	5.86	0.14
		100	6.65	0.08
	CNN	20	15.35	0.92
		50	7.48	0.24
		100	9.05	0.18
MNIST	MLP	20	16.03	0.95
		50	9.72	0.28
		100	13.90	0.15
	CNN	20	306.19	33.60
		50	24.26	1.09
		100	6.14	0.09
CIFAR10	VGG19	20	4.16	0.21

4.2 Communication Saved

Unlike uplink compression, the number of bits saved from downlink compression is related to the number of participating workers. If N workers contributed sparse gradients with K_{uplink} non-zero indices, then the gradient sent back by the server after aggregation is a sparse gradient with at most $K_{\text{uplink}}N$ non-zero indices, and applying top_K sparsification in the downlink will compress the gradient to at most $K_{\text{downlink}}/(K_{\text{uplink}}N)$ of its size. We measure the percentage of non-zero indices in the sum of gradients from the workers, as shown in Figure 4 and supplemental material A.3.4. For all experiments, we see that the fraction approaches $K_{\text{uplink}}N/d$ as the number of iterations increase, showing that the compression rate of the downlink top_K compressor is almost as large as possible.

The time it takes to transfer a gradient from worker-to-server then server-to-worker for unidirectional compression is

$$\alpha_1 + 2K_{\text{uplink}}\beta_1 + \alpha_2 + 2NK_{\text{uplink}}\beta_2, \quad (20)$$

and the time it takes to transfer a message in bidirectional compression is

$$\alpha_1 + 2K_{\text{uplink}}\beta_1 + \alpha_2 + 2K_{\text{downlink}}\beta_2, \quad (21)$$

where α_1 is the uplink latency, α_2 is the downlink latency, β_1 is the uplink transfer time for a 32-bit float, and β_2 is the downlink transfer time for a 32-bit float.

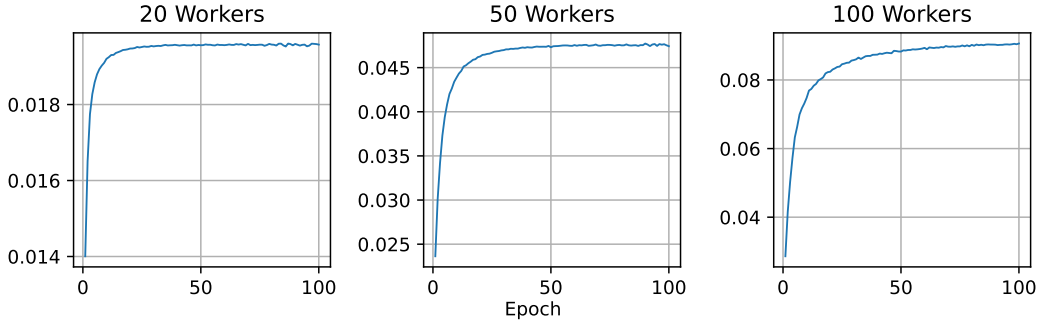


Figure 4: Fraction of non-zero indices after aggregating sparse gradients from workers. Trained on a MLP network using Fashion MNIST dataset. $K_{\text{uplink}} = K_{\text{downlink}} \approx 0.001d$.

5 Conclusion

We demonstrate that bidirectional top_K SGD that can potentially have a tighter convergence bound than unidirectional top_K SGD while providing significant communication benefits. We remove the restriction of Alistarh *et al.*'s non-convex analysis of unidirectional top_K SGD that requires $K > \frac{1}{2}$ [2]. We provide testing across different models, datasets, and number of workers at state-of-the-art sparsification levels [7] to show that bidirectional top_K SGD can converge as well as unidirectional top_K SGD. Our work shows that bidirectional compression should always be used, especially for large number of workers, because server-to-worker communication can be reduced by a factor proportional to N , without affecting convergence speed or accuracy.

References

- [1] Alham Fikri Aji and Kenneth Heafield. Sparse Communication for Distributed Gradient descent. *arXiv preprint arXiv:1704.05021*, 2017.
- [2] Dan Alistarh, Torsten Hoefer, Mikael Johansson, Nikola Konstantinov, Sarit Khirirat, and Cédric Renggli. The Convergence of Sparsified Gradient Methods. *Advances in Neural Information Processing Systems*, 31, 2018.
- [3] Jadhav Ashwin. Federated-Learning-PyTorch. <https://github.com/AshwinRJ/Federated-Learning-PyTorch>, 2019.

- [4] Tal Ben-Nun and Torsten Hoefer. Demystifying Parallel and Distributed Deep Learning: An In-Depth Concurrency Analysis. *ACM Computing Surveys (CSUR)*, 52(4):1–43, 2019.
- [5] Aleksandr Beznosikov, Samuel Horváth, Peter Richtárik, and Mher Safaryan. On Biased Compression for Distributed Learning. *arXiv preprint arXiv:2002.12410*, 2020.
- [6] Léon Bottou, Frank E Curtis, and Jorge Nocedal. Optimization Methods for Large-Scale Machine Learning. *Siam Review*, 60(2):223–311, 2018.
- [7] Mingzhe Chen, Deniz Gündüz, Kaibin Huang, Walid Saad, Mehdi Bennis, Aneta Vulgarakis Feljan, and H Vincent Poor. Distributed Learning in Wireless Networks: Recent Progress and Future Challenges. *IEEE Journal on Selected Areas in Communications*, 2021.
- [8] Li Deng. The MNIST Database of Handwritten Digit Images for Machine Learning Research [Best of the Web]. *IEEE Signal Processing Magazine*, 29(6):141–142, 2012.
- [9] Facebook. Pytorch Examples. <https://github.com/pytorch/examples/blob/main/mnist/main.py>, 2020.
- [10] Joeri Hermans. *On Scalable Deep Learning and Parallelizing Gradient Descent*. PhD thesis, Maastricht U., 2017.
- [11] Sai Praneeth Karimireddy, Quentin Rebjock, Sebastian Stich, and Martin Jaggi. Error Feedback Fixes SignSGD and Other Gradient Compression Schemes. In *International Conference on Machine Learning*, pages 3252–3261. PMLR, 2019.
- [12] Alex Krizhevsky, Geoffrey Hinton, et al. Learning Multiple Layers of Features from Tiny Images. 2009.
- [13] Kuang Liu. Pytorch-Cifar. <https://github.com/kuangliu/pytorch-cifar>, 2021.
- [14] Xiaorui Liu, Yao Li, Jiliang Tang, and Ming Yan. A double residual compression algorithm for efficient distributed learning. In *International Conference on Artificial Intelligence and Statistics*, pages 133–143. PMLR, 2020.
- [15] Constantin Philippenko and Aymeric Dieuleveut. Bidirectional compression in heterogeneous settings for distributed or federated learning with partial participation: Tight convergence guarantees. *arXiv preprint arXiv:2006.14591*, 2020.
- [16] Constantin Philippenko and Aymeric Dieuleveut. Preserved Central Model for Faster Bidirectional Compression in Distributed Settings. *Advances in Neural Information Processing Systems*, 34, 2021.
- [17] Felix Sattler, Simon Wiedemann, Klaus-Robert Müller, and Wojciech Samek. Robust and Communication-Efficient Federated Learning from Non-IID Data. *IEEE Transactions on Neural Networks and Learning Systems*, 31(9):3400–3413, 2019.
- [18] Karen Simonyan and Andrew Zisserman. Very Deep Convolutional Networks for Large-Scale Image Recognition. *arXiv preprint arXiv:1409.1556*, 2014.
- [19] Sebastian U Stich, Jean-Baptiste Cordonnier, and Martin Jaggi. Sparsified SGD with Memory. *Advances in Neural Information Processing Systems*, 31, 2018.
- [20] Hanlin Tang, Chen Yu, Xiangru Lian, Tong Zhang, and Ji Liu. Doublesqueeze: Parallel Stochastic Gradient Descent with Double-Pass Error-Compensated Compression. In *International Conference on Machine Learning*, pages 6155–6165. PMLR, 2019.
- [21] Han Xiao, Kashif Rasul, and Roland Vollgraf. Fashion-MNIST: a Novel Image Dataset for Benchmarking Machine Learning Algorithms, 2017.
- [22] Hang Xu, Chen-Yu Ho, Ahmed M Abdelmoniem, Aritra Dutta, El Houcine Bergou, Konstantinos Karatsenidis, Marco Canini, and Panos Kalnis. Compressed Communication for Distributed Deep Learning: Survey and Quantitative Evaluation. Technical report, 2020.
- [23] Shuai Zheng, Ziyue Huang, and James Kwok. Communication-Efficient Distributed Blockwise Momentum SGD with Error-Feedback. *Advances in Neural Information Processing Systems*, 32, 2019.

A Appendix

A.1 Toy Example

Consider solving the distributed problem with 3 workers

$$\min_{w \in \mathbb{R}^{100}} F(w) \triangleq \frac{1}{3} \sum_{q=1}^3 F^q(w),$$

where

$$\begin{aligned} F^1(w) &\triangleq \frac{1}{2}(w - \vec{1})^T(w - \vec{1}), \\ F^2(w) &\triangleq \frac{1}{2}(w - \vec{5})^T(w - \vec{5}), \\ F^3(w) &\triangleq \frac{1}{2}(w - \vec{10})^T(w - \vec{10}). \end{aligned}$$

The minimum value of $F(w)$ is $\frac{6100}{9}$, when $w = \frac{\vec{16}}{3}$. We initialize $w_0 \in \mathbb{R}^{100}$ generated from $\mathcal{N}(20, 1)$ with random seed 10, and run Algorithm 1 and 2 with $K = 1$. Note that since we can solve the gradient, there is no stochastic element.

Both unidirectional (uplink) and bidirectional top_K SGD oscillates periodically at a distance away from the optimal value. However, bidirectional top_K SGD converges closer to the F^* than unidirectional uplink top_K SGD, which is counter-intuitive, since we should be losing information by adding downlink compression.

We provide an explanation of this by observing the gradients from each worker in unidirectional top_K SGD at $t = 210$. a_t^q from each worker q in line 3 of Algorithm 1 is shown in Figure 5. We note that the non-zero components from the sum of top_K updates, $\sum_{i=1}^3 \text{Top}_K(a_t^q)$, shown in Figure 6 is very different from the corresponding components in the sum of updates, $\sum_{i=1}^3 a_t^q$, shown in Figure 7. This happens because the components from worker 1 and worker 3 have opposite signs. If the largest gradient component from workers 1 and 3 do not have the same index, then $\sum_{i=1}^3 \text{Top}_K(a_t^q)$ will be far from $\sum_{i=1}^3 a_t^q$. In our example, the norm of the difference between the full update and unidirectional (uplink) update step is greater than the norm of the difference between the full and the bidirectional update. Specifically, for unidirectional (uplink) top_K SGD, at $t = 210$,

$$\left\| \sum_{q=1}^3 a_t^q - \sum_{q=1}^3 \text{Top}_K(a_t^q) \right\|_2 = 21.80,$$

while

$$\left\| \sum_{q=1}^3 a_t^q - \text{Top}_K\left(\sum_{q=1}^3 \text{Top}_K(a_t^q)\right) \right\|_2 = 21.54,$$

showing that adding downlink top_K sparsification brings the update closer to the uncompressed update. While applying downlink compression causes the gradient to lose information, it also causes the gradient to lose “bad” information. This motivates us to split the error into 2 parts for unidirectional top_K SGD,

$$\begin{aligned} &\left\| \sum_{q=1}^N p_q a_t^q - \sum_{q=1}^N p_q \text{Top}_K(a_t^q) \right\|_2 \\ &\leq \left\| \sum_{q=1}^N p_q a_t^q - \text{Top}_K\left(\sum_{q=1}^N p_q a_t^q\right) \right\|_2 + \left\| \text{Top}_K\left(\sum_{q=1}^N p_q a_t^q\right) - \sum_{q=1}^N p_q \text{Top}_K(a_t^q) \right\|_2. \end{aligned} \tag{22}$$

One benefit of the new representation is that it has nice physical meaning. The first norm is the error inherent to the compressor and can be bounded by γ -approximate compressor defined

in Assumption (3.2), and the second norm is the error that comes from the distributed system, which occurs when the gradients from the local workers are not representative of the global gradient. Plotting $\|\text{Top}_K(\sum_{q=1}^N p_q a_t^q) - \sum_{q=1}^N p_q \text{Top}_K(a_t^q)\|_2$ and $\|\text{Top}_K(\delta_{t-1} + \sum_{q=1}^N p_q a_t^q) - \text{Top}_K(\delta_{t-1} + \sum_{q=1}^N p_q \text{Top}_K(a_t^q))\|_2$ in Figure 9 for bidirectional and unidirectional downlink top_K SGD, we see that adding a downlink top_K compressor to unidirectional top_K SGD can reduce the distributed error. Intuitively, the update step is noisy, and applying an extra top_K compression would reduce the noise.

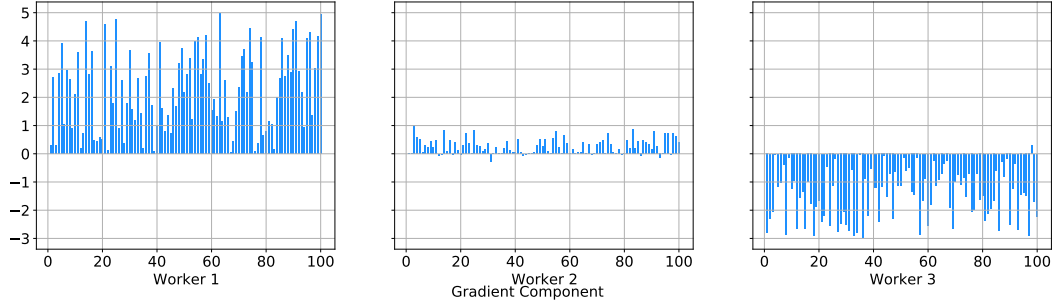


Figure 5: a_t^q from each worker at $t = 300$ for unidirectional top_K SGD.

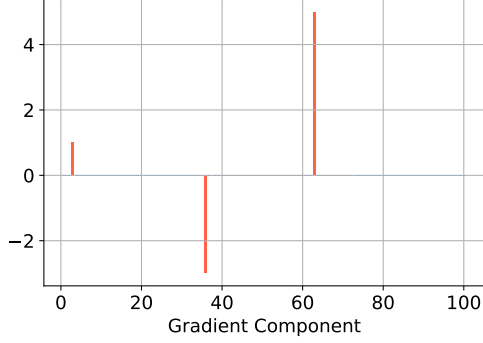


Figure 6: $\sum_{q=1}^N \text{Top}_K(a_t^q)$ at $t = 300$ for unidirectional top_K SGD.

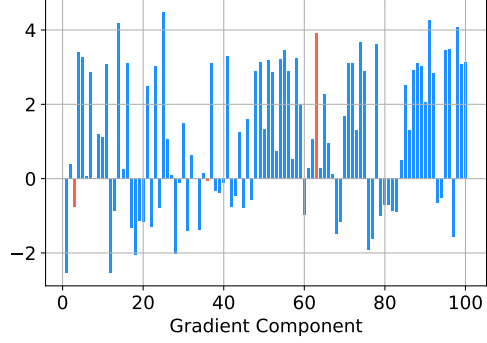


Figure 7: $\sum_{q=1}^N a_t^q$ at $t = 300$ for unidirectional top_K SGD.

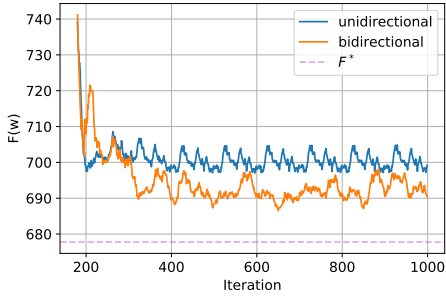


Figure 8: Convergence of unidirectional vs bidirectional top_K SGD run with $K = 1$ and $\alpha = 0.01$.

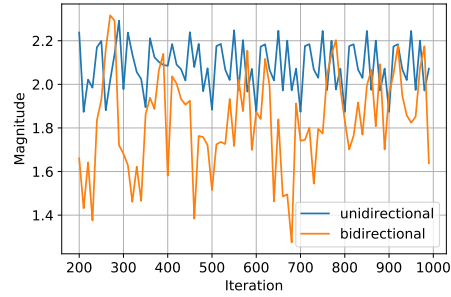


Figure 9: Average $\|\text{Top}_K(\sum_{q=1}^N p_q a_t^q) - \sum_{q=1}^N \text{Top}_K(p_q a_t^q)\|_2$ values every 10 iterations for unidirectional top_K SGD and average $\|\text{Top}_K(\delta_{t-1} + \sum_{q=1}^N p_q a_t^q) - \text{Top}_K(\delta_{t-1} + \sum_{q=1}^N \text{Top}_K(p_q a_t^q))\|_2$ values every 10 iterations for bidirectional top_K SGD.

A.2 Learning Rates

Table 2: Learning rate chosen for all models.

Dataset	Model	Workers	unidirectional lr	bidirectional lr	SGD lr
Fashion MNIST	MLP	20	0.08	0.08	0.06
		50	0.13	0.12	0.07
		100	0.22	0.22	0.08
	CNN	20	0.09	0.08	0.06
		50	0.12	0.11	0.07
		100	0.14	0.2	0.08
MNIST	MLP	20	0.06	0.09	0.03
		50	0.17	0.18	0.1
		100	0.17	0.24	0.1
	CNN	20	0.08	0.09	0.05
		50	0.14	0.16	0.07
		100	0.09	0.16	0.07
CIFAR10	VGG19	20	0.05	0.05	0.05

A.3 Experiment Figures

A.3.1 Testing Accuracy and Training Loss

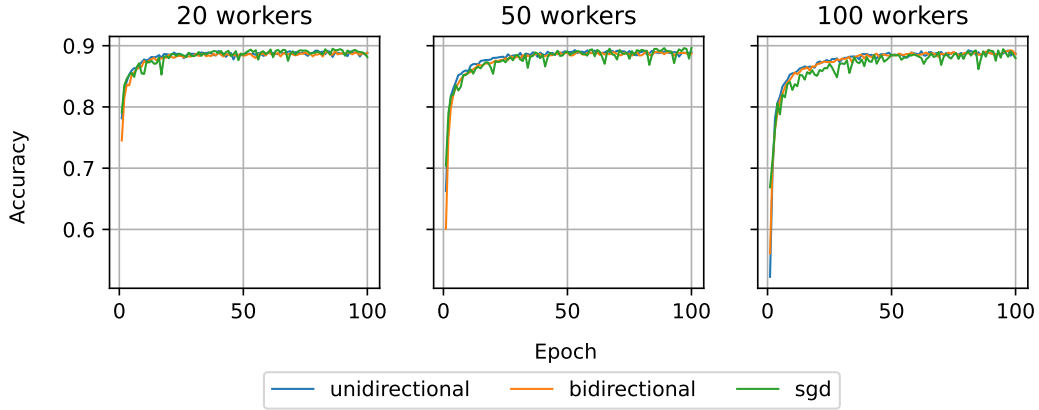


Figure 10: Comparison of testing accuracy for MLP model trained on Fashion MNIST data for unidirectional top_K , bidirectional top_K and vanilla SGD. Trained on batch size 10. $K_{\text{downlink}} = K_{\text{uplink}} \approx 0.001d$ for bidirectional. $K_{\text{uplink}} \approx 0.001d$ for unidirectional.

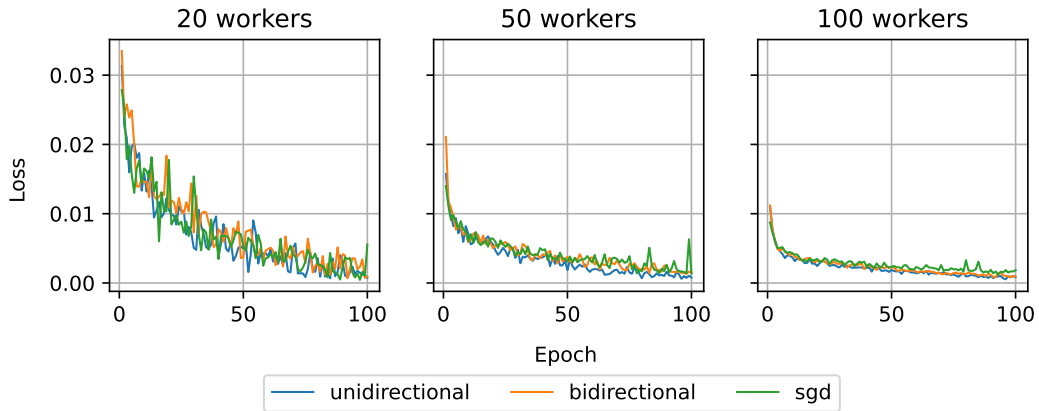


Figure 11: Comparison of training loss for MLP model trained on Fashion MNIST data for unidirectional top_K , bidirectional top_K and vanilla SGD. Trained on batch size 10. $K_{\text{downlink}} = K_{\text{uplink}} \approx 0.001d$ for bidirectional. $K_{\text{uplink}} \approx 0.001d$ for unidirectional.

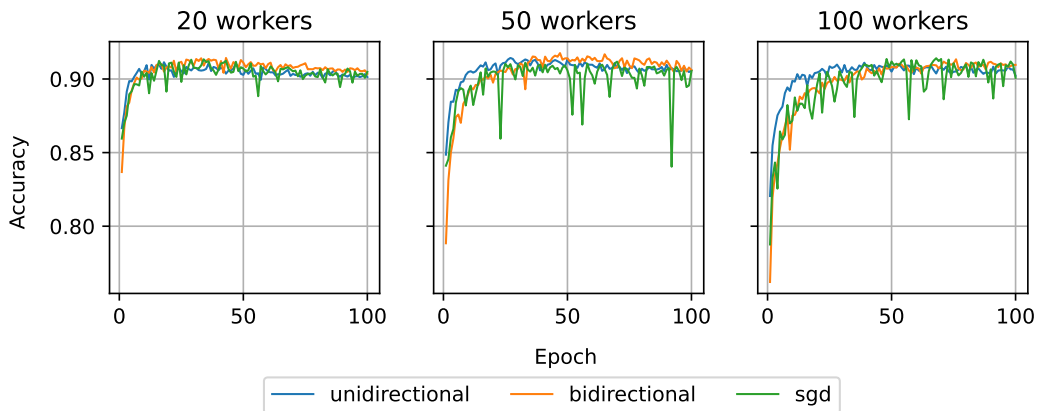


Figure 12: Comparison of testing accuracy from training CNN model on Fashion MNIST data for unidirectional top_K , bidirectional top_K and vanilla SGD. Trained on batch size 10. $K_{\text{downlink}} = K_{\text{uplink}} \approx 0.001d$ for bidirectional. $K_{\text{uplink}} \approx 0.001d$ for unidirectional.

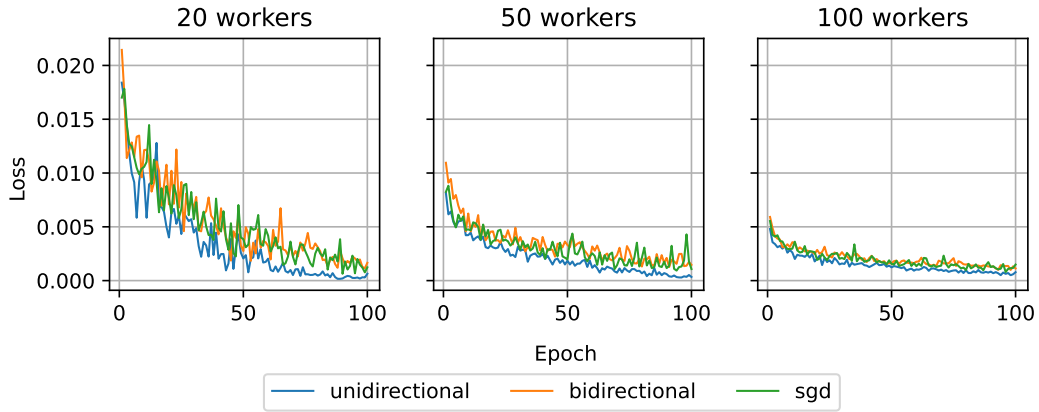


Figure 13: Comparison of training loss from training CNN model on Fashion MNIST data for unidirectional top_K , bidirectional top_K and vanilla SGD. Trained on batch size 10. $K_{\text{downlink}} = K_{\text{uplink}} \approx 0.001d$ for bidirectional. $K_{\text{uplink}} \approx 0.001d$ for unidirectional.

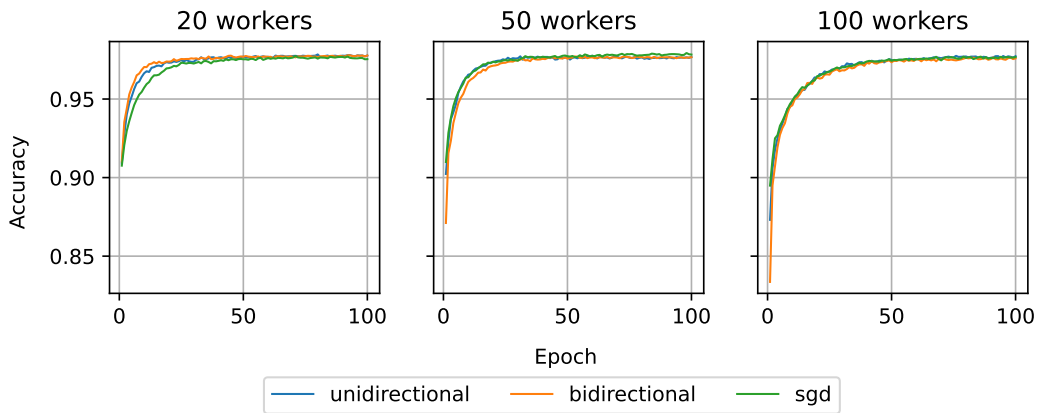


Figure 14: Comparison of testing accuracy from training MLP model on MNIST data for unidirectional top_K , bidirectional top_K and vanilla SGD. Trained on batch size 10. $K_{\text{downlink}} = K_{\text{uplink}} \approx 0.001d$ for bidirectional. $K_{\text{uplink}} \approx 0.001d$ for unidirectional.

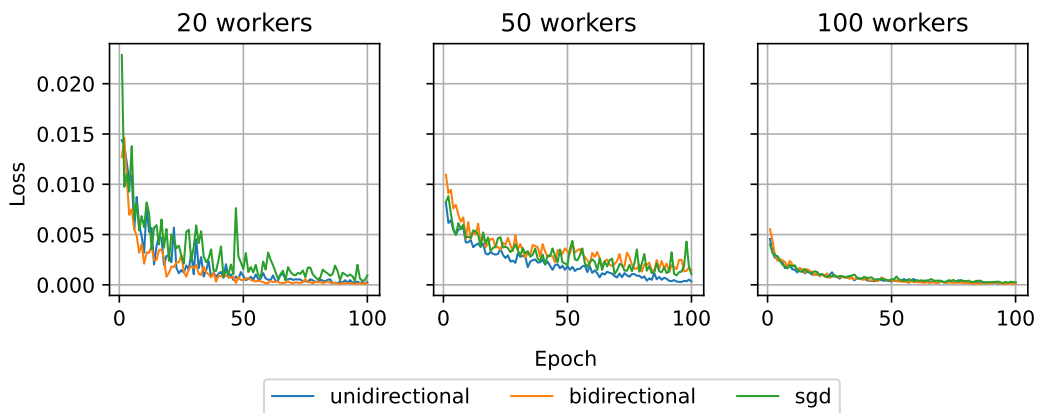


Figure 15: Comparison of training loss from training MLP model on MNIST data for unidirectional top_K , bidirectional top_K and vanilla SGD. Trained on batch size 10. $K_{\text{downlink}} = K_{\text{uplink}} \approx 0.001d$ for bidirectional. $K_{\text{uplink}} \approx 0.001d$ for unidirectional.

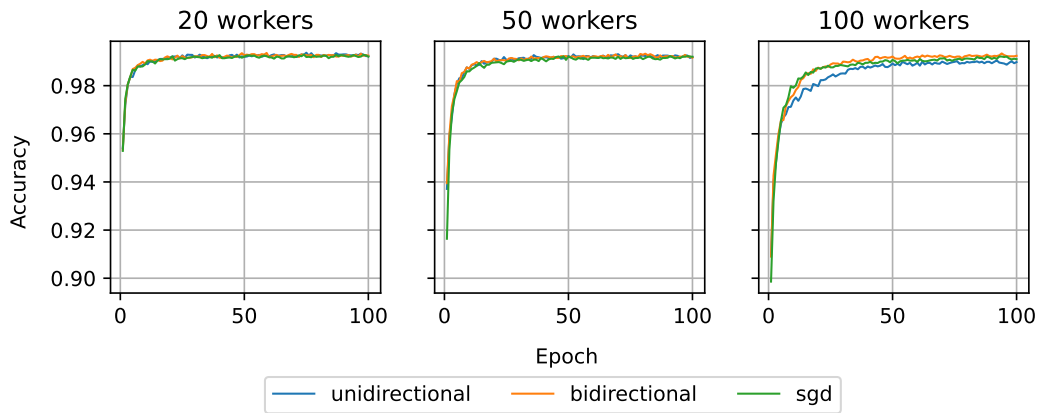


Figure 16: Comparison of testing accuracy from training CNN model on MNIST data for unidirectional top_K , bidirectional top_K and vanilla SGD. Trained on batch size 10. $K_{\text{downlink}} = K_{\text{uplink}} \approx 0.001d$ for bidirectional. $K_{\text{uplink}} \approx 0.001d$ for unidirectional.

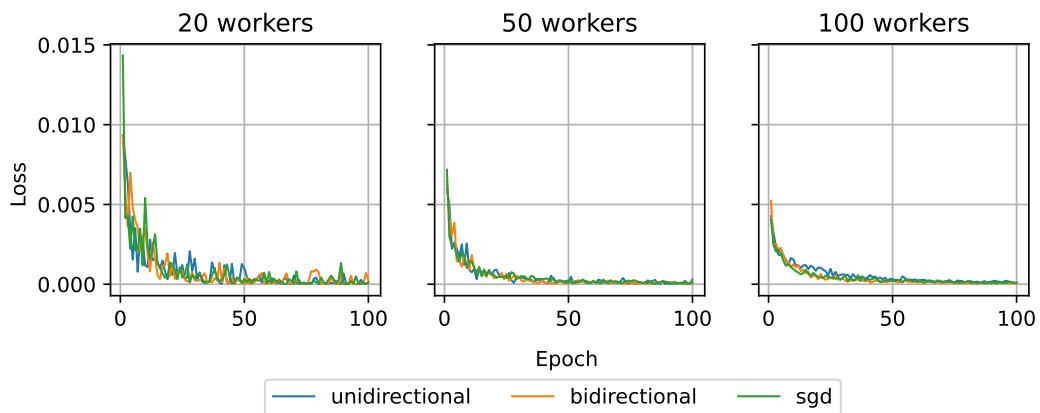


Figure 17: Comparison of training loss from training CNN model on MNIST data for unidirectional top_K , bidirectional top_K and vanilla SGD. Trained on batch size 10. $K_{\text{downlink}} = K_{\text{uplink}} \approx 0.001d$ for bidirectional. $K_{\text{uplink}} \approx 0.001d$ for unidirectional.

A.3.2 ρ vs $\hat{\rho}$ Values

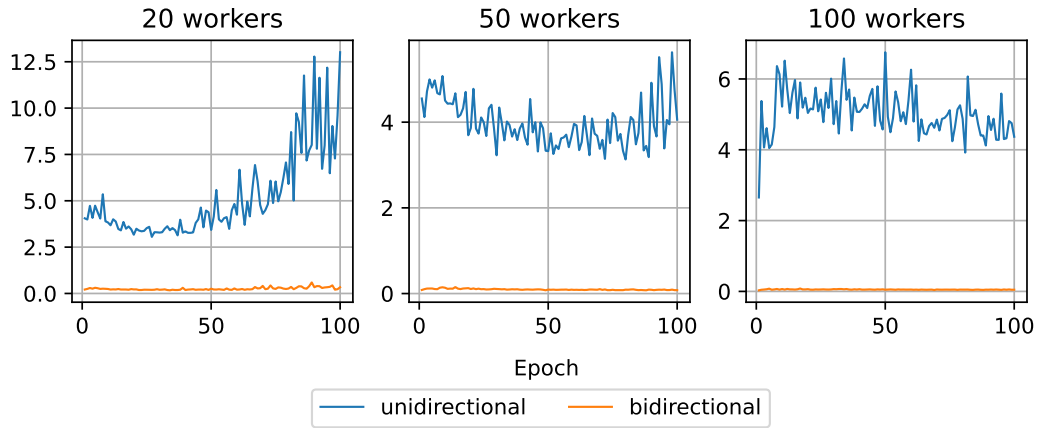


Figure 18: Comparison of ρ vs $\hat{\rho}$ values from training MLP model on Fashion MNIST data for unidirectional top_K and bidirectional top_K . Models trained on batch size 10. $K_{\text{downlink}} = K_{\text{uplink}} \approx 0.001d$ for bidirectional. $K_{\text{uplink}} \approx 0.001d$ for unidirectional.

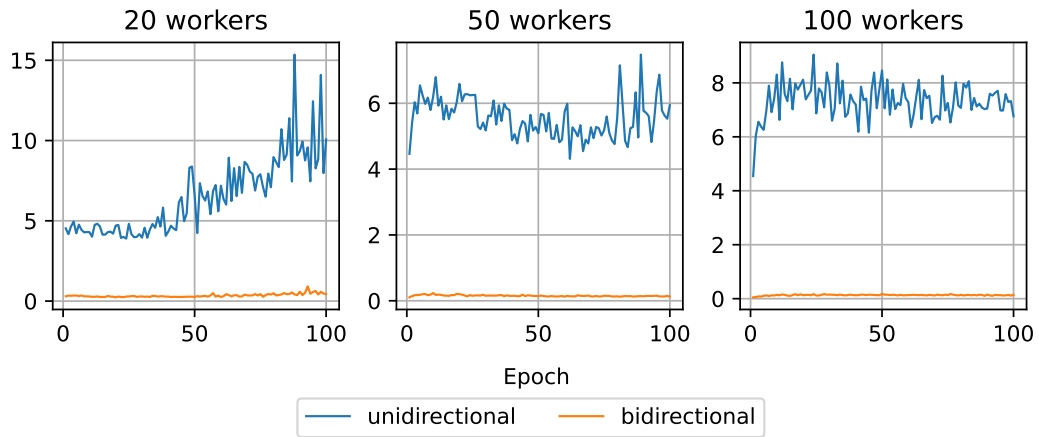


Figure 19: Comparison of ρ vs $\hat{\rho}$ values from training CNN model on Fashion MNIST data for unidirectional top_K and bidirectional top_K . Models trained on batch size 10. $K_{\text{downlink}} = K_{\text{uplink}} \approx 0.001d$ for bidirectional. $K_{\text{uplink}} \approx 0.001d$ for unidirectional.

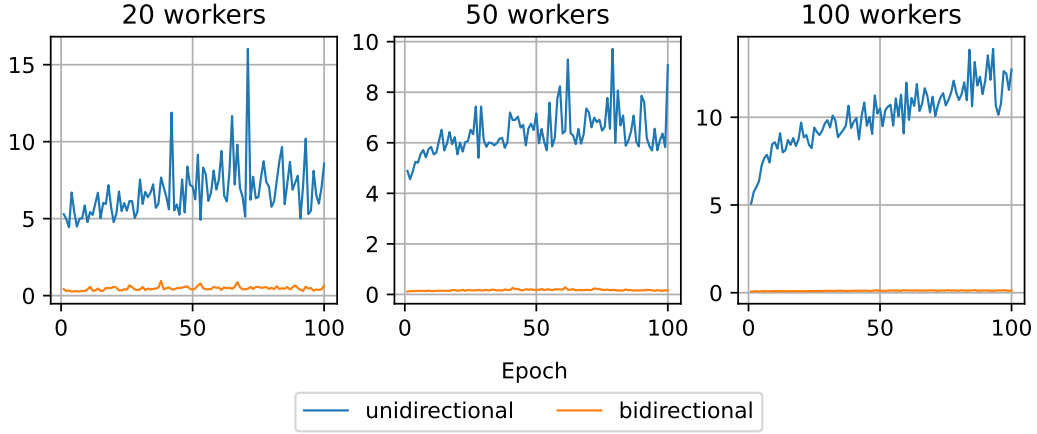


Figure 20: Comparison of ρ vs $\hat{\rho}$ values from MLP Model trained on MNIST data for unidirectional top_K and bidirectional top_K . Models trained on batch size 10. $K_{\text{downlink}} = K_{\text{uplink}} \approx 0.001d$ for bidirectional. $K_{\text{uplink}} \approx 0.001d$ for unidirectional.

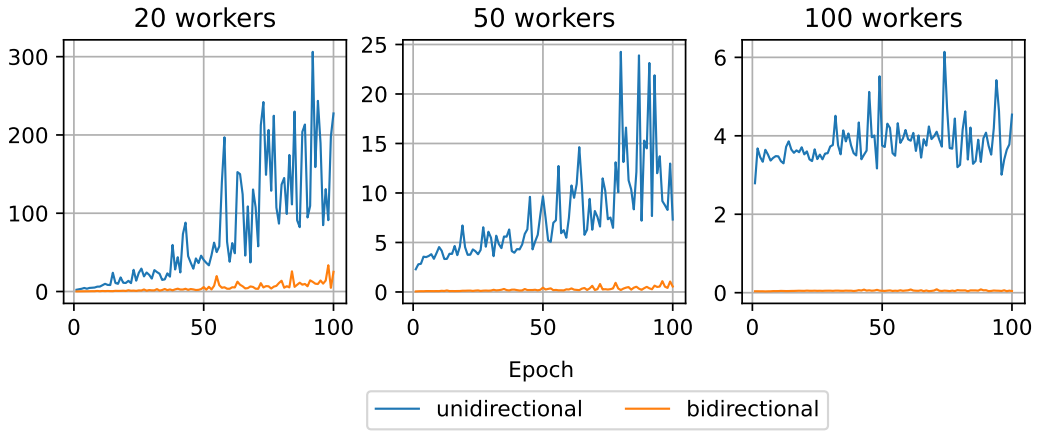


Figure 21: Comparison of ρ vs $\hat{\rho}$ values from CNN Model trained on MNIST data for unidirectional top_K and bidirectional top_K . Models trained on batch size 10. $K_{\text{downlink}} = K_{\text{uplink}} \approx 0.001d$ for bidirectional. $K_{\text{uplink}} \approx 0.001d$ for unidirectional.

A.3.3 $1 - \gamma$ values

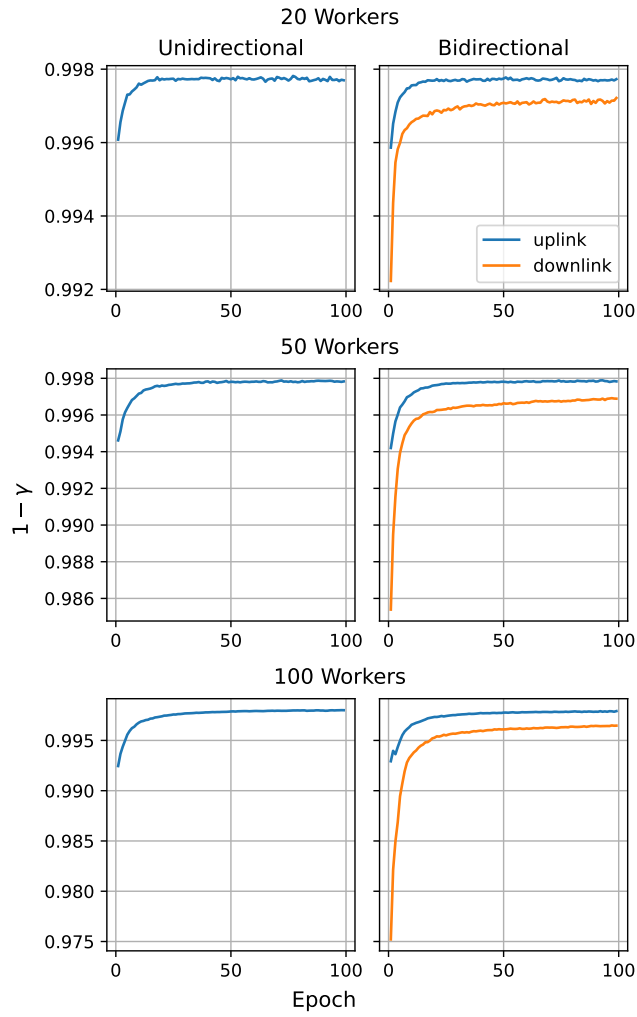


Figure 22: Largest $1 - \gamma$ value in each epoch of a MLP model trained with unidirectional and bidirectional top_K SGD on Fashion MNIST dataset.

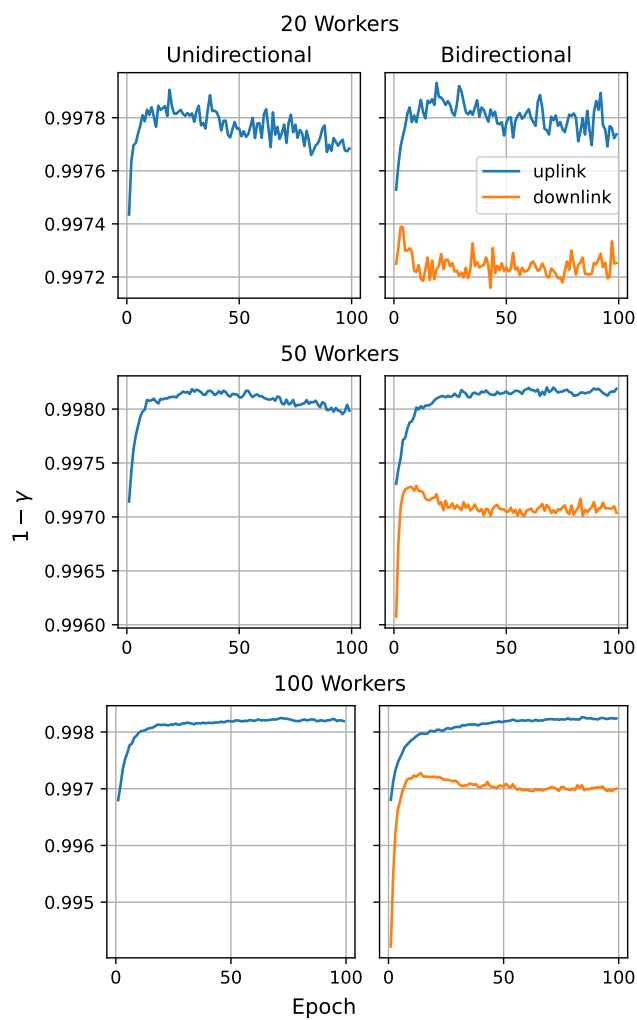


Figure 23: Largest $1 - \gamma$ value in each epoch of a CNN model trained with unidirectional and bidirectional top_K SGD on a Fashion MNIST dataset.

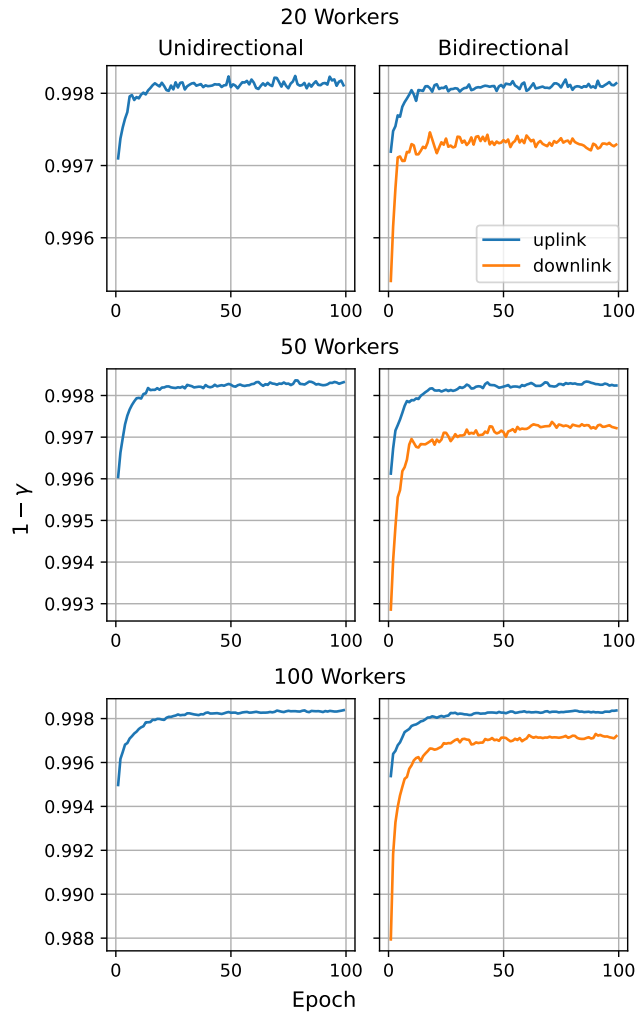


Figure 24: Largest $1 - \gamma$ value in each epoch of a MLP model trained with unidirectional and bidirectional top_K SGD on a MNIST dataset.

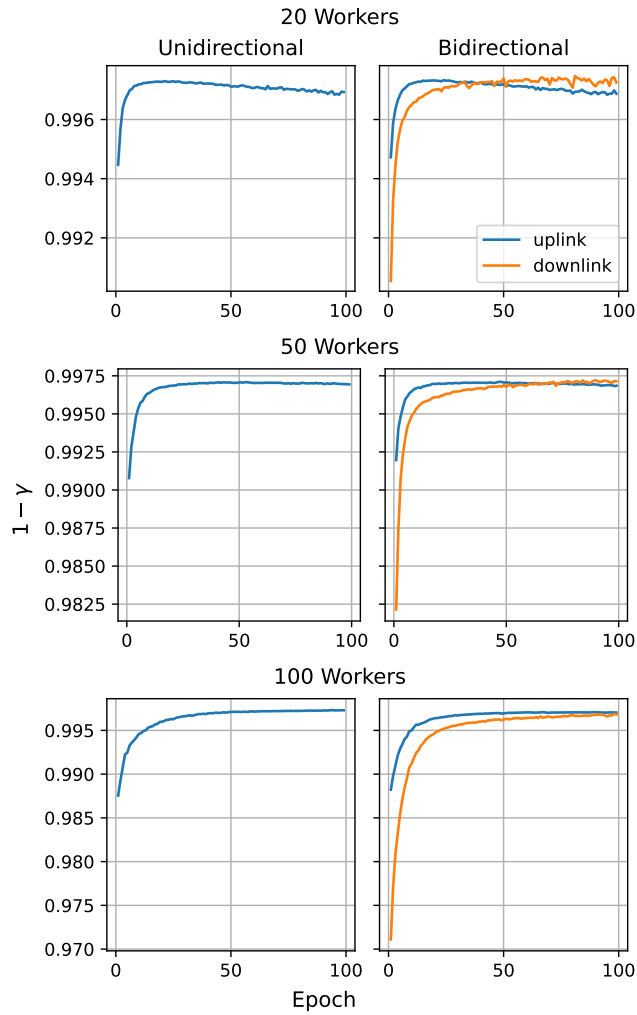


Figure 25: Largest $1 - \gamma$ value in each epoch of a CNN model trained with unidirectional and bidirectional top_K SGD on a MNIST dataset.

A.3.4 Fraction of Non-Zero Indices in Gradient After Server Aggregation

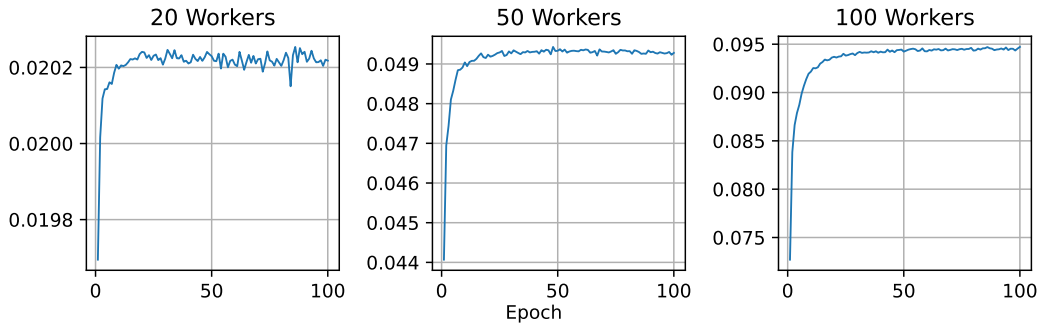


Figure 26: Percent of non-zero indices after aggregating sparse gradients from workers. Trained on a CNN Model using Fashion MNIST dataset. $K_{\text{uplink}} = K_{\text{downlink}} \approx 0.001d$.

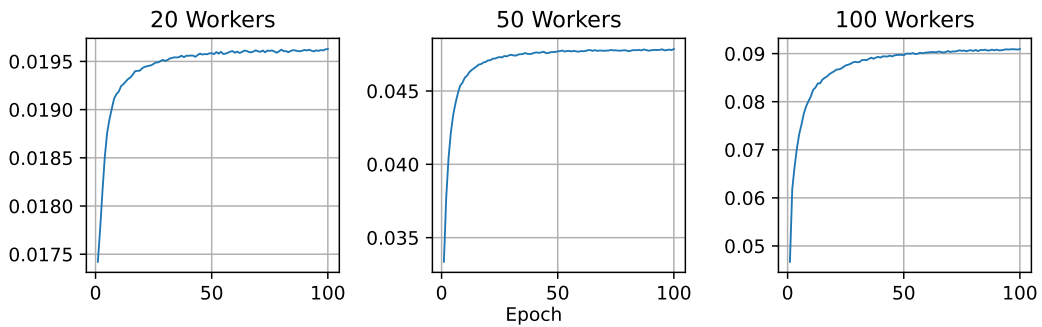


Figure 27: Percent of non-zero indices after aggregating sparse gradients from workers. Trained on a MLP Model using MNIST dataset. $K_{\text{uplink}} = K_{\text{downlink}} \approx 0.001d$.

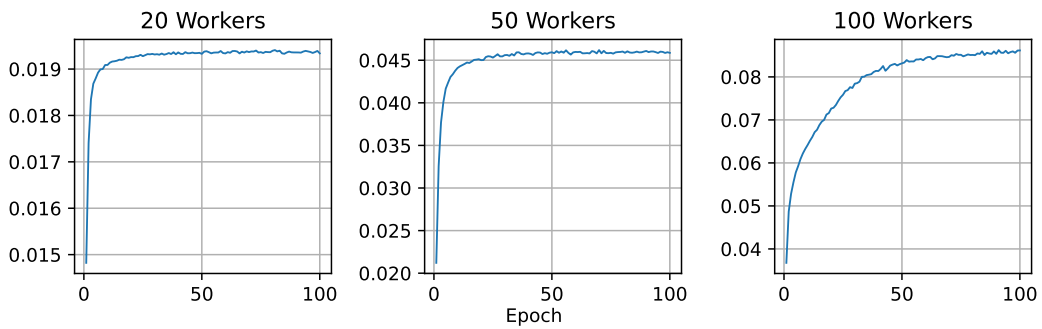


Figure 28: Fraction of non-zero indices after aggregating sparse gradients from workers. Trained on a CNN Model using MNIST dataset. $K_{\text{uplink}} = K_{\text{downlink}} \approx 0.001d$.